Influence of 8-oxoguanine on the thermal stability of G-quadruplex DNA and the interactions with the FANCJ AKKQ peptide

Laura Campbell[1,#a], Kaitlin Lowran[1,#b], Emma Cismas[1], Colin G. Wu[1*]

[1] Department of Chemistry, Oakland University, Rochester, Michigan, United States of America

[#a] Current Address: Department of Biochemistry, University of Wisconsin-Madison, Madison, Wisconsin, United States of America

[#b] Current Address: Institute of Environmental Health Sciences, Wayne State University, Detroit, Michigan, United States of America

* Corresponding author

E-mail: colinwu@oakland.edu (CGW)

Abstract

Guanine-rich nucleic acid sequences can adopt G-quadruplex (G4) structures, which pose barriers to DNA replication and repair. The FANCJ helicase contributes to genome stability by resolving these structures, a function linked to its G4-binding site that features an AKKQ amino acid motif. This site is thought to recognize oxidatively damaged G4, specifically those containing 8-oxoguanine (8oxoG) modifications. We hypothesize that FANCJ AKKQ recognition of 8oxoG-modified G4s (8oxoG4s) depends on the sequence context, the position of the lesion within the G4, and overall structural stability. Using fluorescence spectroscopy, we measured the binding affinities of a FANCJ AKKQ peptide for G4s formed by $(GGGT)_4$, $(GGGTT)_4$, and $(TTAGGG)_4$ sequences. G4 conformation and thermal stability were assessed by circular dichroism spectroscopy. Each sequence was modified to include a single 8oxoG at the first (8oxo1), third (8oxo3), or fifth (8oxo5) guanine position. In potassium chloride (KCl), the most destabilized structures were $(GGGT)_4$ 8oxo1, $(GGGTT)_4$ 8oxo1, and $(TTAGGG)_4$ 8oxo5. In sodium chloride (NaCl), the most destabilized were $(GGGT)_4$ 8oxo1, $(GGGTT)_4$ 8oxo5, and $(TTAGGG)_4$ 8oxo5. FANCJ AKKQ binding affinities varied according to damage position and sequence context, with notable differences for $(GGGT)_4$ in KCl and $(TTAGGG)_4$ in NaCl. These findings support a model in which FANCJ binding to G4 and

34 8oxoG4 structures is modulated by both the oxidative damage position and the G4 local
35 sequence environment.
36

37 Introduction

38 G-quadruplexes (G4s) are stable secondary structures that are formed by guanine-
39 rich nucleic-acids. G4 DNA structures arise from intramolecular Hoogsteen hydrogen
40 bonding within single-stranded (ss) DNA containing four tracts of three or more
41 consecutive guanines [1]. Monovalent cations further stabilize G4s by centrally
42 coordinating the guanine tetrads, with potassium (K^+) and sodium (Na^+) ions being the
43 most biologically relevant. Among them, potassium ions generally confer greater stability
44 to G4s [2-4].

45 The canonical sequence motif for G4 formation is $(GGGN_{1\text{-}7})_4$, where N denotes
46 any intervening nucleotides [5]. This has led to an estimate of over 400,000 potential G4
47 forming sequences being identified in the human genome [6]. G4s can adopt multiple
48 topologies—parallel, antiparallel, or hybrid—depending on the nucleotide sequence and
49 solution conditions (Fig 1) [4, 7]. These G4 conformations are defined by how the loop
50 regions ($N_{1\text{-}7}$) connect the guanine tracts [8, 9], and can be distinguished using circular
51 dichroism (CD) spectroscopy [10]. The spatial arrangements of G4s are biologically

52 significant, as many G4-binding proteins have a preference for specific topologies; the

53 Pif1 helicase, for example, binds and unfolds antiparallel G4s [11-15].

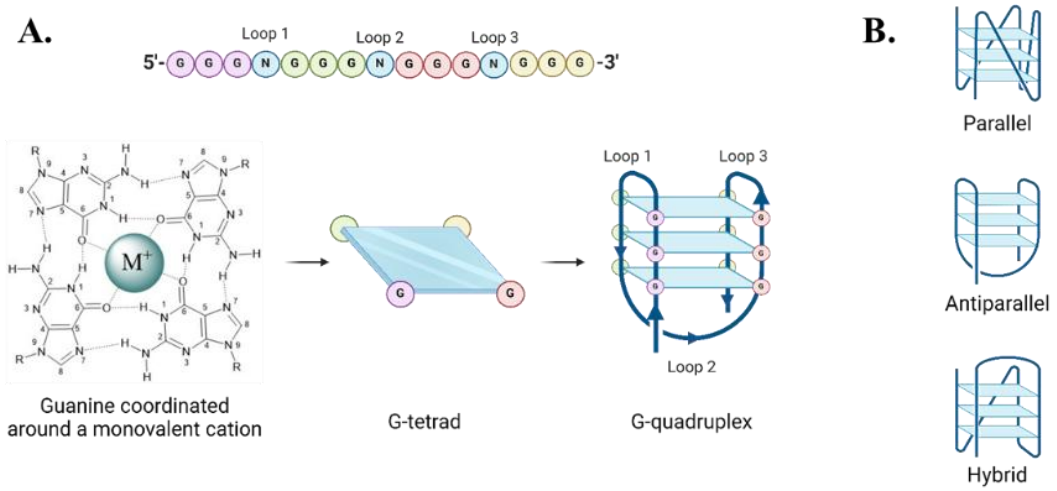

54

55 **Fig 1. G-quadruplex formation and conformations.** (A) Formation of a G4 structure. (B)
56 Graphic representation of three different intra-strand G4 conformations.

57 G4 structures are enriched in genomic regions involved in transcriptional

58 regulation, RNA processing, and telomere maintenance [5, 16-20]. While G4s may play

59 regulatory roles, their accumulation can be deleterious to cells, as they can impede

60 replication, repair, and transcription [16]. Consequently, G4s have emerged as attractive

61 therapeutic targets. The G4-stabilizing compound CX-5461 induces DNA breaks and

62 induces replication fork collapse, highlighting its potential in targeting tumor cells [21].

63 A key vulnerability of G4-forming regions is their susceptibility to oxidative stress.

64 Guanine has the lowest oxidation potential of the four DNA bases, and its propensity to

65 be oxidized increases when the guanines are stacked or arranged consecutive runs

66 [22,23]. Oxidation of guanine can produce 8-oxoguanine (8oxoG), a lesion that can
67 mispair with either adenine or cytosine, leading to G to T transversion mutations if left
68 unrepaired [24,25]. Although G4s containing 8oxoG (i.e. 8oxoG4s) can still form, the
69 lesion reduces their stability, rendering them susceptible to nuclease digestion and
70 potentially leading to telomere shortening [26,27]. Nuclear magnetic resonance (NMR)
71 studies have shown that 8oxoG incorporation into human telomeric G4s alters their
72 topology by changing the guanine glycosidic angles from anti to syn configuration [26].
73 Thus, G4s and 8oxoG4s must be resolved in dividing cells to maintain genomic integrity.
74 FANCJ (Fanconi anemia complementation group J) is one of several proteins that
75 can unfold G4s in human cells. As an iron-sulfur helicase, FANCJ participates in the
76 repair of interstrand DNA crosslinks as part of the Fanconi anemia pathway [28].
77 Mutations in FANCJ are associated with increased cancer risk and Fanconi anemia [28-
78 30]. FANCJ contributes to genome stability not only through DNA repair, but also by
79 resolving G4 structures that impede replication [31-35]. Upon encountering a G4-stalled
80 replication fork, FANCJ binds and unwinds the G4, allowing DNA replication to resume,
81 potentially through the recruitment of translesion polymerases such as REV1 [36] (Fig 2).

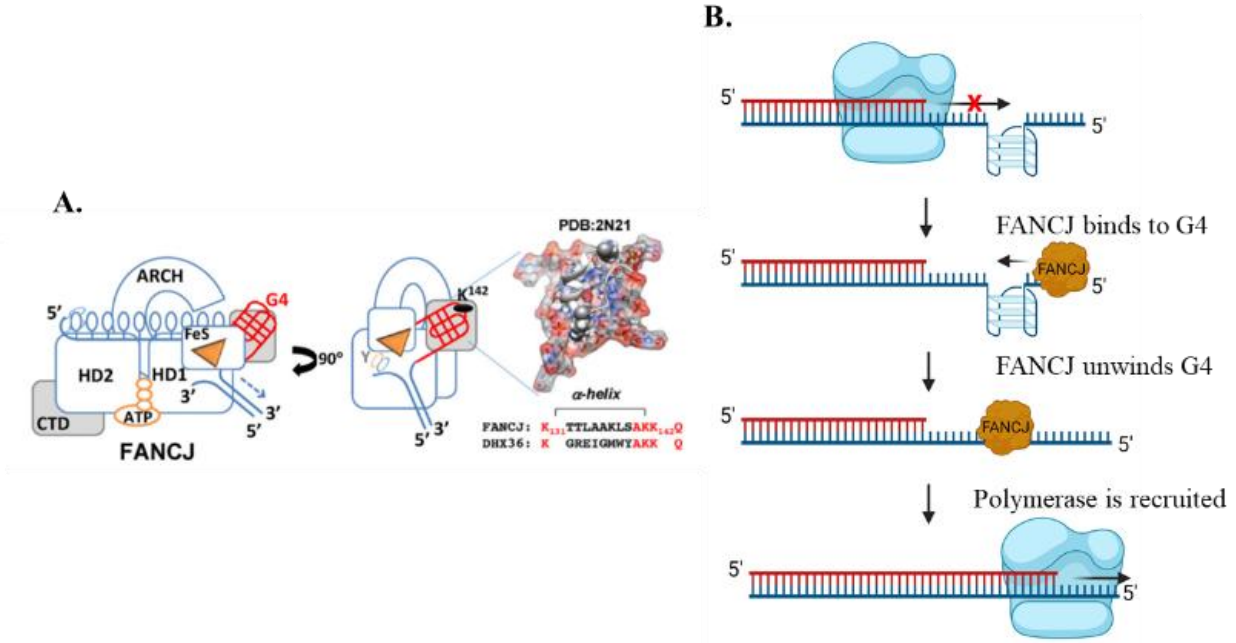

Fig 2. Molecular models of FANCJ. (A) FANCJ possesses a G4 recognition site capable of binding G4s, and an AKKQ motif similar in structure and sequence to the AKKQ binding motif found in G4-binding protein RHAU [11, 37]. (B) The current model for FANCJ-supported DNA replication in G4-rich sequences. Upon reaching a G4 structure, the DNA polymerase stalls. FANCJ binds to the G4 structure to unwind it and another polymerase is recruited to continue DNA replication.

Interestingly, a related RNA helicase RHAU (also known as DHX36), recognizes G4 structures via an AKKQ motif, where the tandem lysine residues facility G4-binding [11, 37]. FANCJ contains a similar G4 binding site with an AKKQ motif centered at lysines K141 and K142 [33]. This motif enables FANCJ to anchor to both G4 and 8oxoG4 DNA as shown in our previous work (Fig 3) [36]. In this study, we further characterize the sequence- and damage-dependent recognition of G4 and 8oxoG4 by the FANCJ AKKQ motif by exploring how intervening loop length and guanine oxidation at distinct positions affect FANCJ AKKQ peptide binding and G4 stability.

Fig 3. Map of FANCJ. The AKKQ sequence (amino acids 129-147) has been highlighted.

Results

G-quadruplex conformation and thermal stability

Circular dichroism (CD) spectroscopy was used to assess the conformation and thermal stability of twelve G4 sequences in buffers containing either KCl and NaCl. G4 structures exhibit distinct CD signatures based on their topology, enabling discrimination between parallel, antiparallel, and hybrid configurations (Fig 4A) [9, 10]. CD experiments were performed as a function of temperature to derive the T_m (melting temperature), which reflects the thermal stability of each G4 substrate (Fig 4B and 4C) [38].

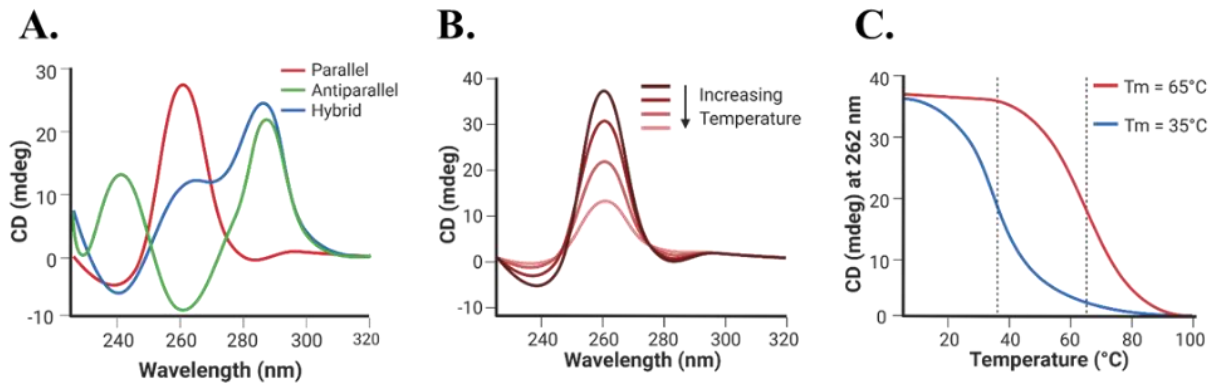

Fig 4. CD spectroscopy cartoons. (A) Graphic representation of CD spectra for parallel, antiparallel, and hybrid G4 conformations. Parallel conformations have a maximum at 262 nm and a minimum at 240 nm. Antiparallel conformations give two peak signals near 295 nm and 240 nm, and a minimum at 260 nm. Hybrid conformations show a peak at 295 nm, a shoulder around 260 nm, and a minimum at 240 nm. (B) Graphic representation of the CD spectra of a parallel G4 conformation as a function of temperature. (C) Graphic representation of a thermal melt graph of two G4s.

Three G4-forming sequences were selected based on their biological relevance and loop length: $(GGGT)_4$, a compact parallel G4-forming aptamer for HIV-1 integrase that possesses a single thymine base for the ssDNA loop [7, 39]; $(TTAGGG)_4$, is the canonical human telomeric repeat sequence that has a TTA loop between the guanine tracts [19]; $(GGGTT)_4$, an artificial sequence with an intermediate loop length (TT) compared to the other two substrates. Oxidative damage was introduced by substate an 8oxoG at the first (8oxo1), third (8oxo3), or fifth (8oxo5) guanine position of each sequence (Fig 5), thereby targeting each of the three tetrad stacks.

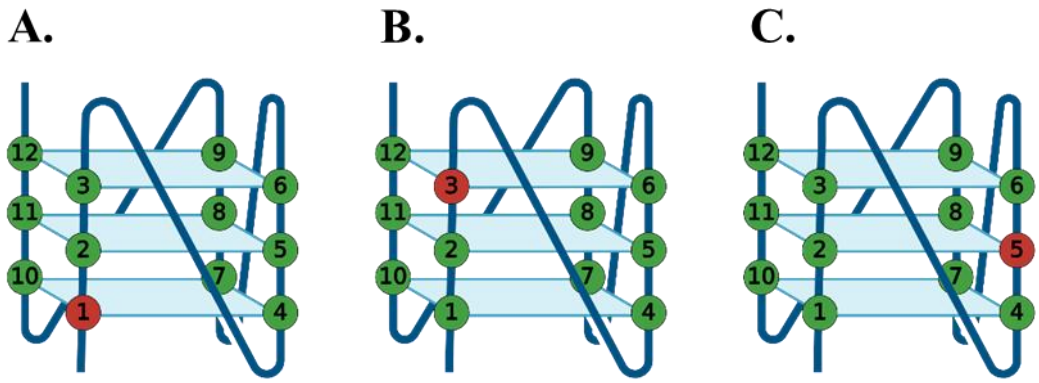

Fig 5. Graphic representation of a parallel G4 conformation. An 8oxoG-modified base has been substituted at the (A) first guanine (8oxo1), (B) third guanine (8oxo3), and (C) fifth guanine (8oxo5).

In 150 mM KCl, all $(GGGT)_4$ sequences formed a parallel quadruplex (Fig 6A), with only subtle changes to the CD spectra when 8oxoG was incorporated. Due to temperature limitations of the instrument, the native sequence was not fully unfolded even at 95 °C, and its T_m was estimated to be > 88.4 ± 8.4 °C (Table 1), consistent with prior reports [7,36]. All 8oxoG substitutions led to reduced thermal stability, with the largest destabilization observed for $(GGGT)_4$ 8oxo1 ($\Delta T_m = -19.0 \pm 8.4$ °C) and the smallest for 8oxo3 ($\Delta T_m = -8.1 \pm 8.4$ °C).

Table 1. Summary of G4 conformation and melting temperature in 150 mM KCl

Name	Conformation	T_m (°C)	ΔT_m (°C)
$(GGGT)_4$	Parallel	> 88.4 ± 8.4	-
$(GGGT)_4$ 8oxo1	Parallel	69.4 ± 0.6	-19.0 ± 8.4

$(GGGT)_4$ 8oxo3	Parallel	80.3 ± 0.4	-8.1 ± 8.4
$(GGGT)_4$ 8oxo5	Parallel	71.6 ± 0.4	-16.8 ± 8.4
$(GGGTT)_4$	Parallel	83.5 ± 0.7	-
$(GGGTT)_4$ 8oxo1	Parallel	52.0 ± 1.4	-31.5 ± 1.6
$(GGGTT)_4$ 8oxo3	Antiparallel	57.2 ± 0.3	-26.3 ± 0.7
$(GGGTT)_4$ 8oxo5	Parallel	55.9 ± 0.3	-27.6 ± 0.8
$(TTAGGG)_4$	Hybrid	62.5 ± 0.5	-
$(TTAGGG)_4$ 8oxo1	Hybrid-esque	54.5 ± 0.5	-8.0 ± 0.7
$(TTAGGG)_4$ 8oxo3	Antiparallel	49.5 ± 0.3	-13.0 ± 0.6
$(TTAGGG)_4$ 8oxo5	Hybrid-esque	38.9 ± 0.6	-23.6 ± 0.8

135

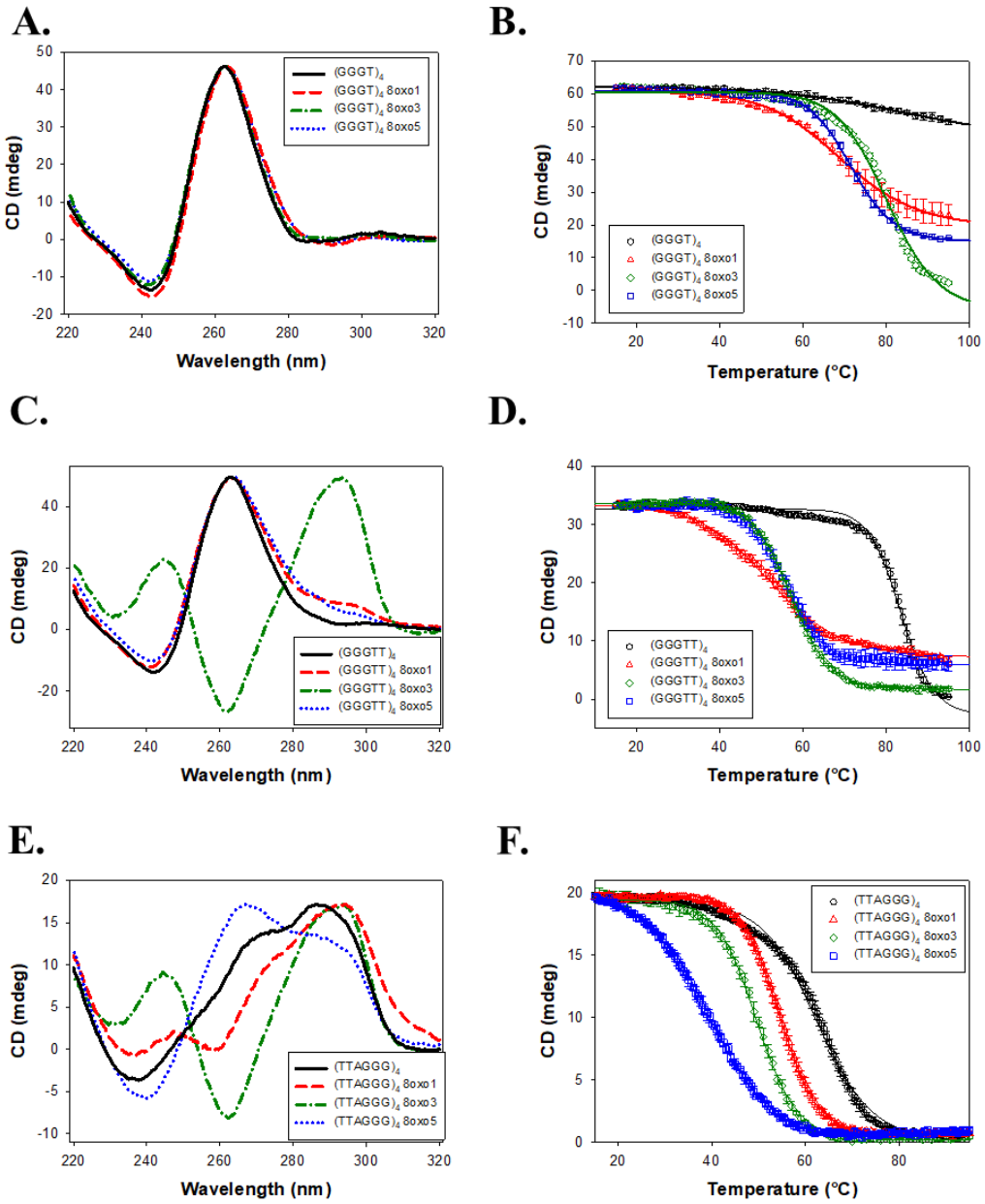

Fig 6. Experiments performed in the presence of 150 mM KCl. (A) CD spectra of $(GGGT)_4$, $(GGGT)_4$ 8oxo1, $(GGGT)_4$ 8oxo3, and $(GGGT)_4$ 8oxo5 taken from 320 to 220 nm. (B) Temperature melt of same sequences seen in 6A. Melt taken at 262 nm from 15 to 95 °C. (C) CD spectra of $(GGGTT)_4$, $(GGGTT)_4$ 8oxo1, $(GGGTT)_4$ 8oxo3, and $(GGGTT)_4$ 8oxo5 taken from 320 to 220 nm. (D) Temperature melt of same sequences seen in 6C. Melt taken at 262 nm for all sequences except $(GGGTT)_4$ 8oxo3, which was taken at 295 nm. (E) CD spectra of $(TTAGGG)_4$, $(TTAGGG)_4$ 8oxo1, $(TTAGGG)_4$ 8oxo3, and $(TTAGGG)_4$ 8oxo5 taken from 320 to 220 nm. (F) Temperature melt of the same sequences seen in 6E. Melt taken at 295 nm.

146 $(GGGTT)_4$ also adopted a parallel conformation in KCl (Fig 6C). While 8oxo1 and
147 8oxo5 substitutions retained a predominantly parallel fold with minor spectral shifts, the
148 8oxo3 variant formed an antiparallel quadruplex. The native $(GGGTT)_4$ had a T_m of
149 83.5 ± 0.7 °C. 8oxoG destabilized the structure in a similar trend, with 8oxo1 producing
150 the largest drop ($\Delta T_m = -31.5 \pm 1.6$ °C) and 8oxo3 the least ($\Delta T_m = -26.3 \pm 0.7$ °C).

151 $(TTAGGG)_4$ folded as a hybrid G4 in KCl (Fig 6E). $(TTAGGG)_4$ 8oxo1 and
152 $(TTAGGG)_4$ 8oxo5 sequences also formed hybrid conformations, although with
153 significant structural changes. $(TTAGGG)_4$ 8oxo1 had a significant right shift in the 295
154 nm peak and a double trough at 260 and 240 nm. $(TTAGGG)_4$ 8oxo5 experienced
155 depression in its peak at 295 nm and an increase in its shoulder at 260 nm and trough at
156 240 nm. Similar to $(GGGTT)_4$ 8oxo3, the $(TTAGGG)_4$ 8oxo3 sequence changed to the
157 antiparallel conformation. $(TTAGGG)_4$ had a T_m of 62.5 ± 0.5 °C (Fig 6F; Table 1).
158 Consistent with a previous study, $(TTAGGG)_4$ 8oxo5 had the highest decrease in thermal
159 stability of ΔT_m = -23.6 ± 0.8 °C while $(TTAGGG)_4$ 8oxo1 had the lowest change in thermal
160 stability of ΔT_m = -8.0 ± 0.7 °C [27].

161 In NaCl-containing buffer, $(GGGT)_4$ maintained a parallel configuration across all
162 damaged variants (Fig 7A). The native sequence had a T_m of 70.3 ± 0.7 °C. Substitution
163 with 8oxoG again decreased thermal stability, most notably at the 8oxo1 position
164 ($\Delta T_m = -27.8 \pm 0.9$ °C), with 8oxo3 being least affected ($\Delta T_m = -13.9 \pm 0.8$ °C) (Table 2).

165 **Table 2. Summary of G4 conformation and melting temperature in 150 mM NaCl**

Name	Conformation	T_m (°C)	Δ T_m (°C)
$(GGGT)_4$	Parallel	70.3 ± 0.7	-
$(GGGT)_4$ 8oxo1	Parallel	42.5 ± 0.5	-27.8 ± 0.9
$(GGGT)_4$ 8oxo3	Parallel	56.4 ± 0.4	-13.9 ± 0.8
$(GGGT)_4$ 8oxo5	Parallel	44.0 ± 0.3	-26.3 ± 0.8
$(GGGTT)_4$	Parallel	44.8 ± 1.2	-
$(GGGTT)_4$ 8oxo1	Antiparallel	47.2 ± 0.3	2.4 ± 1.2
$(GGGTT)_4$ 8oxo3	Antiparallel	44.6 ± 0.2	-0.2 ± 1.2
$(GGGTT)_4$ 8oxo5	Hybrid-esque	27.5 ± 0.9	-17.3 ± 1.4
$(TTAGGG)_4$	Antiparallel	52.1 ± 0.3	-
$(TTAGGG)_4$ 8oxo1	Antiparallel	47.8 ± 0.6	-4.3 ± 0.7
$(TTAGGG)_4$ 8oxo3	Antiparallel	42.2 ± 0.7	-9.9 ± 0.8
$(TTAGGG)_4$ 8oxo5	Antiparallel	33.3 ± 0.4	-18.8 ± 0.5

166

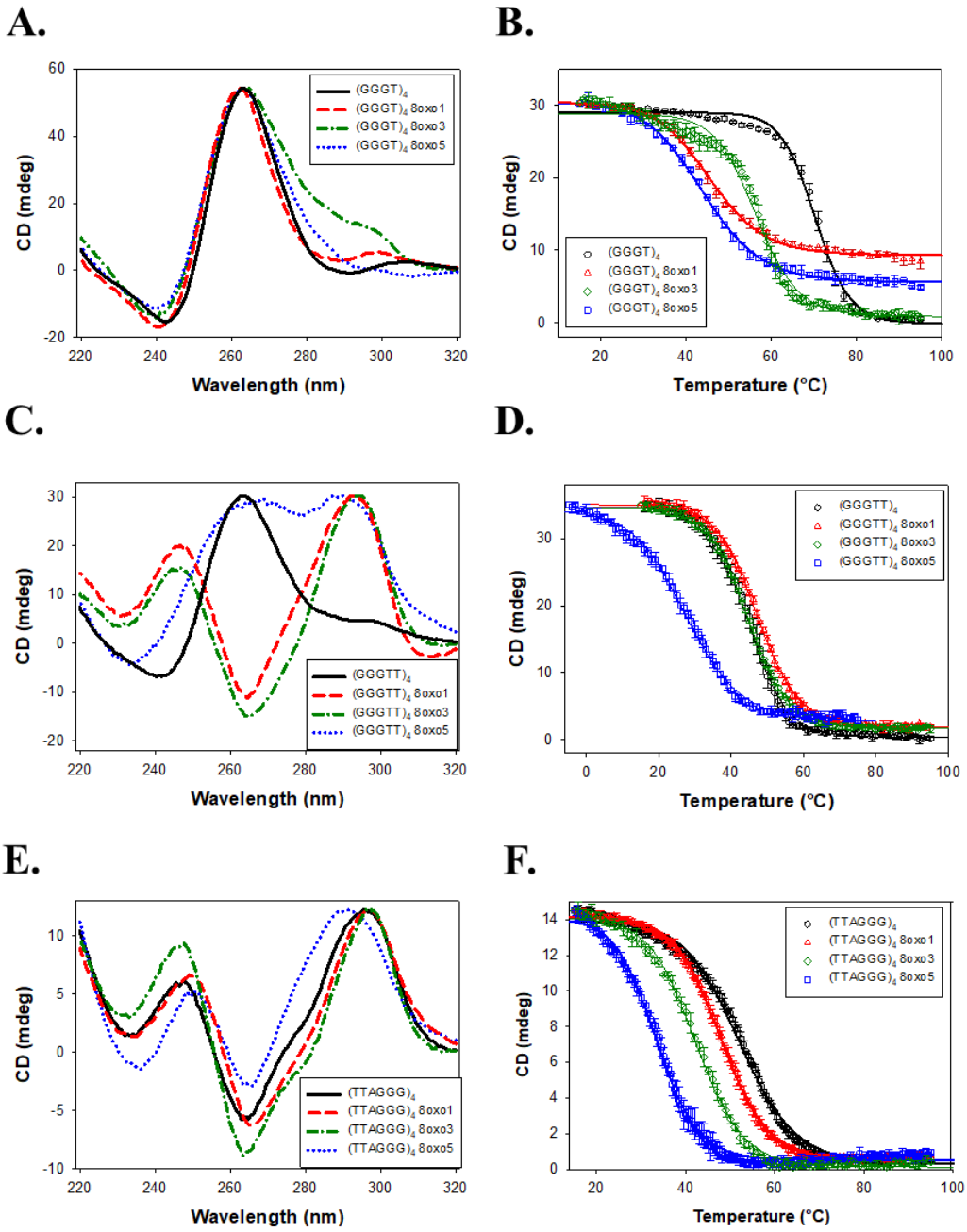

Fig 7. Experiments performed in the presence of 150 mM NaCl. (A) CD spectra of $(GGGT)_4$, $(GGGT)_4$ 8oxo1, $(GGGT)_4$ 8oxo3, and $(GGGT)_4$ 8oxo5 taken from 320 to 220 nm. (B) Temperature melt of same sequences as seen in 7A. Melt taken at 262 nm from 15 to 95 °C. (C) CD spectra of $(GGGTT)_4$, $(GGGTT)_4$ 8oxo1, $(GGGTT)_4$ 8oxo3, and $(GGGTT)_4$ 8oxo5 taken from 320 to 220 nm. (D) Temperature melt of same sequences as seen in 7C. Melt taken at 262 nm for all sequences except $(GGGTT)_4$ 8oxo3, which was taken at 295 nm. (E) CD spectra of $(TTAGGG)_4$, $(TTAGGG)_4$ 8oxo1, $(TTAGGG)_4$ 8oxo3, and

175 $(TTAGGG)_4$ 8oxo5 taken from 320 to 220 nm. (F) Temperature melt of the same sequences
176 as seen in 7E. Melt taken at 295 nm.
177

178 $(GGGTT)_4$ retained a parallel conformation in NaCl, but all three 8oxoG4 variants
179 underwent structural transitions: 8oxo1 and 8oxo3 shifted to antiparallel conformations,
180 and 8oxo5 adopted a hybrid-like structure (Fig 7C). Surprisingly, 8oxo1 showed a slight
181 increase in thermal stability ($\Delta T_m = +2.4 \pm 1.2$ °C), while 8oxo3 had a negligible effect
182 ($\Delta T_m = -0.2 \pm 1.2$ °C). In contrast, 8oxo5 was the most destabilizing ($\Delta T_m = -17.3 \pm 1.4$ °C).
183 The 8oxo5 melting curve was acquired from −5 °C to 75 °C due to incomplete folding at
184 15 °C.

185 $(TTAGGG)_4$ and its 8oxoG4 variants formed antiparallel conformations in NaCl
186 (Fig 7E). The damaged substrates all showed slight peak shifts in the CD spectra
187 compared to the native sequence, indicating slight folding differences. The T_m of
188 $(TTAGGG)_4$ was determined to be 52.1 ± 0.3 °C (Fig 7F; Table 2). Concurrent with
189 previous literature and the KCl data above, $(TTAGGG)_4$ 8oxo5 had the highest decrease
190 in thermal stability of ΔT_m = -18.8 ± 0.5 °C while $(TTAGGG)_4$ 8oxo1 had the lowest of ΔT_m
191 = -4.3 ± 0.7 °C [27].

192 FANCJ AKKQ binding to 8oxoG4s

193 To assess the binding of the FANCJ AKKQ motif to G4 and 8oxoG4 structures,
194 fluorescence titrations were performed using a synthetic peptide with a C-terminal
195 tryptophan (Fig 8A). Tryptophan florescence intensity was quenched upon binding to the
196 DNA substrate, and the extent of quenching was plotted against G4 concentration to

197 produce binding isotherms (Fig 8B). The curves were well-described by a 1:1 binding
198 model (Fig 8C). In 150 mM KCl, the FANCJ AKKQ peptide showed preferential binding
199 to oxidatively damaged $(GGGT)_4$ sequences (Fig 9; Table 3), with the strongest interaction
200 to 8oxo1 ($K = 7.7 \pm 0.7 \times 10^5\ M^{-1}$), followed by 8oxo5 ($K = 4.4 \pm 0.6 \times 10^5\ M^{-1}$), 8oxo3 ($K = 3.2$
201 $\pm 0.1 \times 10^5\ M^{-1}$), and weakest to the undamaged native sequence ($K = 2.7 \pm 0.4 \times 10^5\ M^{-1}$).
202 Because the $(GGGT)_4$ substrate contained only a single thymine nucleotide loop, we next
203 examined the AKKQ peptide binding to G4 structures formed by $(GGGTT)_4$ to test the
204 effects of loop length. All 8oxoG4 variants of this substrate bound to the peptide with
205 similar affinity values ($K \approx 8–9 \times 10^5\ M^{-1}$), which were stronger than its interaction with
206 the undamaged sequence ($K = 6.0 \pm 0.9 \times 10^5\ M^{-1}$). For the human telomeric G4
207 $(TTAGGG)_4$, this substrate contained an incrementally longer TTA loop; the peptide
208 bound with comparable affinity to all variants of this sequence, including the native
209 structure ($K \approx 1.3–1.4 \times 10^6\ M^{-1}$), suggesting a minimal influence of oxidative damage to
210 binding.

211 **Table 3. Summary of FANCJ AKKQ-G4 binding by fluorescence spectroscopy in 150**
212 **mM KCl**

Name	K (M^{-1})	R^2
$(GGGT)_4$	$2.7 \pm 0.4 \times 10^5$	0.997

$(GGGT)_4$ 8oxo1	$7.7 \pm 0.7 \times 10^5$	0.998
$(GGGT)_4$ 8oxo3	$3.2 \pm 0.1 \times 10^5$	0.997
$(GGGT)_4$ 8oxo5	$4.4 \pm 0.6 \times 10^5$	0.997
$(GGGTT)_4$	$6.0 \pm 0.9 \times 10^5$	0.997
$(GGGTT)_4$ 8oxo1	$8.2 \pm 1.0 \times 10^5$	0.997
$(GGGTT)_4$ 8oxo3	$9.6 \pm 1.0 \times 10^5$	0.996
$(GGGTT)_4$ 8oxo5	$9.3 \pm 0.8 \times 10^5$	0.997
$(TTAGGG)_4$	$1.6 \pm 0.7 \times 10^6$	0.996
$(TTAGGG)_4$ 8oxo1	$1.3 \pm 0.4 \times 10^6$	0.997
$(TTAGGG)_4$ 8oxo3	$1.2 \pm 0.1 \times 10^6$	0.996
$(TTAGGG)_4$ 8oxo5	$1.4 \pm 0.5 \times 10^6$	0.997

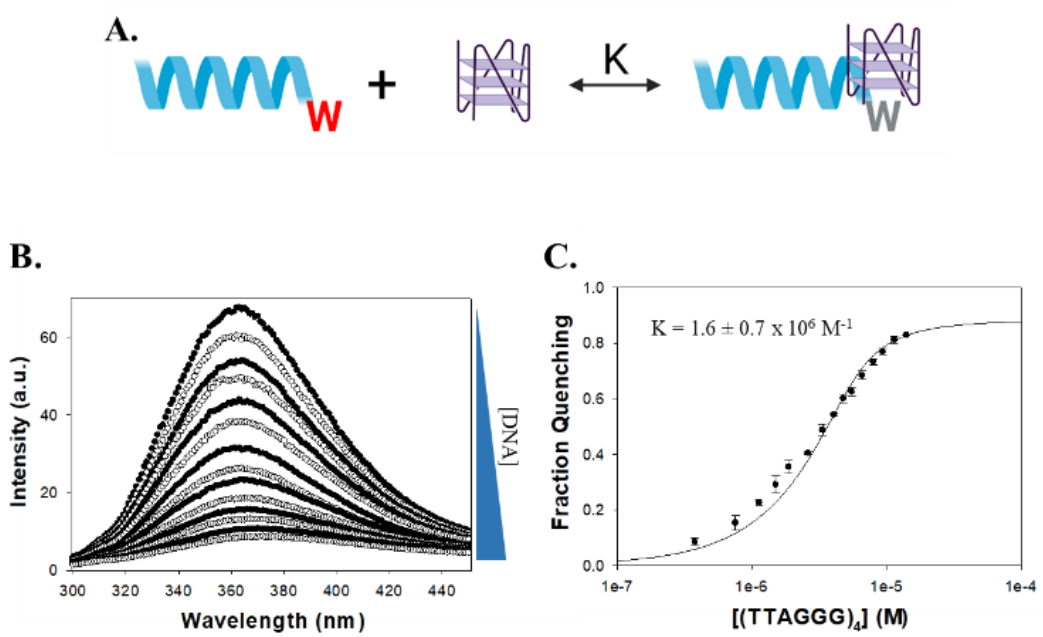

Fig 8. Overview of fluorescence spectroscopy analyses. (A) Molecular model of fluorescence spectroscopy titrations. AKKQ is equipped with a tryptophan residue that fluoresces. When bound to DNA, the residue is quenched and fluorescence intensity decreases. (B) Titration of AKKQ with $(GGGT)_4$. As DNA concentration increases, the peak intensity decreases. (C) Analysis of fluorescence titration. The decrease in integrated peak is plotted as a function of DNA concentration. The resulting isotherm is fit to a 1:1 binding interaction model to generate an equilibrium K value.

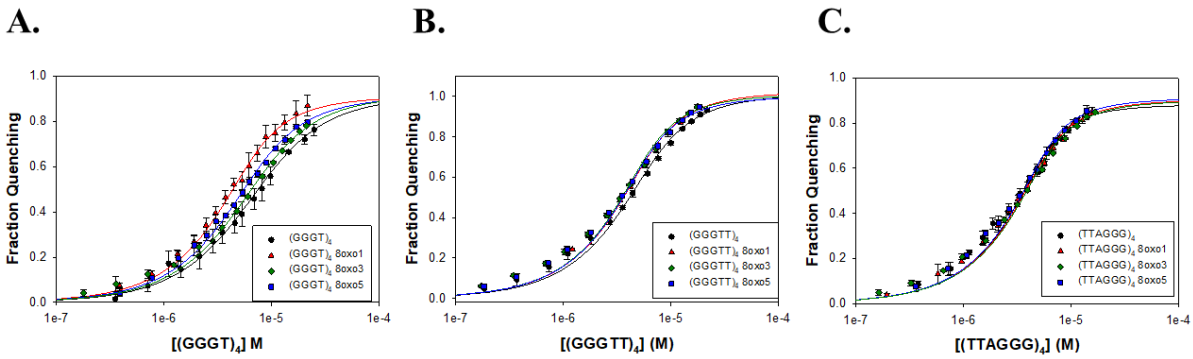

Fig 9. Summary of FANCJ AKKQ-G4 binding in KCl by fluorescence spectroscopy. Trials performed in 20 mM HEPES pH 7.5, 150 mM KCl, 5 mM TCEP, and 5% (v/v) glycerol. (A) FANCJ AKKQ equilibrium binding to $(GGGT)_4$ and its respective 8oxoG4 sequences. (B) FANCJ AKKQ binding to $(GGGTT)_4$ and its respective 8oxoG4 sequences. (C) FANCJ AKKQ binding to $(TTAGGG)_4$ and its respective 8oxoG4 sequences.

230 In NaCl, a similar trend was observed for the $(GGGT)_4$ series (Fig 10; Table 4). The
231 AKKQ peptide bound identically and strongest to 8oxo1 ($3.4 \pm 0.5 \times 10^5$ M^{-1}) and 8oxo5
232 ($3.4 \pm 0.5 \times 10^5$ M^{-1}), followed by 8oxo3 ($2.9 \pm 0.5 \times 10^5$ M^{-1}) and the native sequence ($2.3 \pm$
233 0.3×10^5 M^{-1}). For $(GGGTT)_4$, all sequences exhibited similar binding affinities ($K \approx 4.9$–
234 5.6×10^5 M^{-1}), except for 8oxo1, which showed slightly weaker binding
235 ($K = 3.9 \pm 1.3 \times 10^5$ M^{-1}). For the human telomeric $(TTAGGG)_4$, the highest affinity was
236 observed for 8oxo5 ($K = 1.1 \pm 0.1 \times 10^6$ M^{-1}), followed by the native and 8oxo1 sequences
237 ($K = 6.5 \times 10^5$ M^{-1}), with 8oxo3 binding the weakest ($K = 5.1 \pm 1.1 \times 10^5$ M^{-1}).

238 **Table 4. Summary of FANCJ AKKQ-G4 binding by fluorescence spectroscopy in 150**
239 **mM NaCl**

Name	K (M^{-1})	R^2
$(GGGT)_4$	$2.3 \pm 0.3 \times 10^5$	0.9997
$(GGGT)_4$ 8oxo1	$3.4 \pm 0.5 \times 10^5$	0.9996
$(GGGT)_4$ 8oxo3	$2.9 \pm 0.5 \times 10^5$	0.9994
$(GGGT)_4$ 8oxo5	$3.4 \pm 0.5 \times 10^5$	0.9997
$(GGGTT)_4$	$4.9 \pm 2.0 \times 10^5$	0.9995
$(GGGTT)_4$ 8oxo1	$3.9 \pm 1.3 \times 10^5$	0.9993

$(GGGTT)_4$ 8oxo3	$5.2 \pm 1.7 \times 10^5$	0.9994
$(GGGTT)_4$ 8oxo5	$5.6 \pm 1.1 \times 10^5$	0.9992
$(TTAGGG)_4$	$6.5 \pm 0.6 \times 10^5$	0.9991
$(TTAGGG)_4$ 8oxo1	$6.5 \pm 1.4 \times 10^5$	0.9996
$(TTAGGG)_4$ 8oxo3	$5.1 \pm 1.1 \times 10^5$	0.9998
$(TTAGGG)_4$ 8oxo5	$1.1 \pm 0.1 \times 10^6$	0.9974

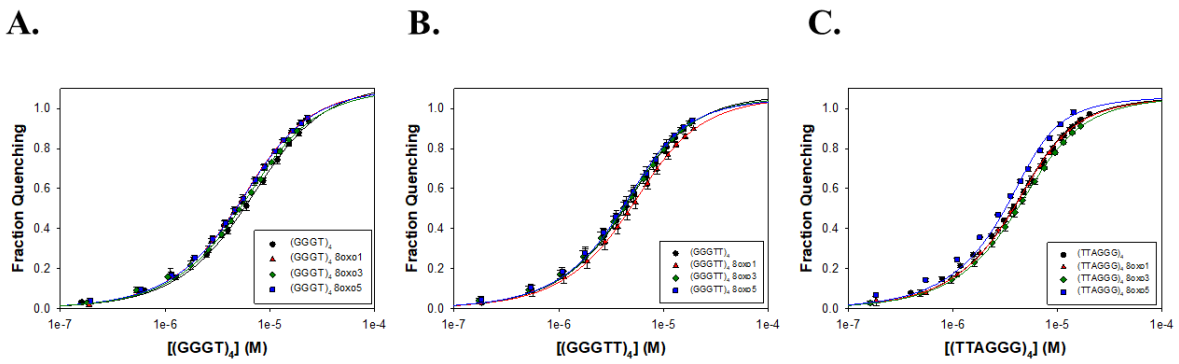

Fig 10. Summary of FANCJ AKKQ-G4 binding in NaCl by fluorescence spectroscopy. Trials performed in 20 mM HEPES pH 7.5, 150 mM NaCl, 5 mM TCEP, and 5% (v/v) glycerol. (A) FANCJ AKKQ binding to $(GGGT)_4$ and respective 8oxoG4 sequences. (B) FANCJ AKKQ binding to $(GGGTT)_4$ and respective 8oxoG4 sequences. (C) FANCJ AKKQ binding to $(TTAGGG)_4$ and respective 8oxoG4 sequences.

Discussion

249 ## G4 conformation and stability

250 Our CD data confirm and expand upon prior studies demonstrating that the
251 human telomeric sequence $(TTAGGG)_4$ adopts hybrid and antiparallel conformations in
252 KCl and NaCl, respectively, and that 8oxoG modifications influence both structure and
253 stability in a position-dependent manner [26,27,41]. As seen by Vorlícková et al, the 8oxo5
254 substitution produced the greatest thermal destabilization in both KCl and NaCl
255 environments, whereas 8oxo1 was the least disruptive [27].

256 This positional effect was also evident in the $(GGGTT)_4$ series in NaCl, where the
257 native sequence maintained a parallel conformation while the 8oxoG-modified variants
258 adopted antiparallel or hybrid structures. In contrast, the $(GGGT)_4$ sequences maintained
259 parallel topology across all variants and salt conditions, with 8oxo1 substitutions
260 consistently producing the greatest destabilization and 8oxo3 the least. A similar pattern
261 was observed for $(GGGTT)_4$ in KCl, where only the 8oxo3 variant deviated from the
262 parallel configuration.

263 Collectively, these findings suggest that the thermal stability of G4 structures in
264 the presence of 8oxoG depends on both the specific guanine position modified and the
265 overall structural context of the G4. In compact, parallel G4s, damage to the first guanine
266 (in the bottom tetrad) was most destabilizing, while damage to the third guanine (top
267 tetrad) had the least effect. Conversely, in more flexible hybrid or antiparallel G4s, the

268 middle tetrad (fifth guanine) was most susceptible to destabilization, while the first
269 guanine remained relatively unaffected. This aligns with earlier NMR-based studies
270 showing significant destabilization and conformational change upon 8oxoG substitution
271 at the fifth guanine in human telomeric G4s [26]. Our data also reinforce the known effects
272 of monovalent cations on G4 stability. Overall, thermal stability was higher in KCl than
273 in NaCl, consistent with the greater stabilizing effect of potassium ions due to their
274 optimal ionic radius for coordinating G-quartets [2–4,42]. Additionally, a trend emerged
275 linking loop length with thermal stability in which shorter loop sequences exhibited
276 higher melting temperatures than longer loops, consistent with previous observations
277 [4,40]. A similar trend was also present but less evident in NaCl buffer, with $(GGGT)_4$ and
278 $(GGGTT)_4$ having the highest and lowest T_m values, respectively.

279 FANCJ AKKQ binding to 8oxoG4s

280 Our fluorescence titration data indicate that the FANCJ AKKQ motif can recognize
281 both native and 8oxoG-modified G4 structures. The binding selectivity was influence by
282 DNA sequence, structural conformation, and position of the 8oxoG.

283 For the $(GGGT)_4$ series, which formed highly stable parallel G4s, AKKQ showed
284 the strongest affinity for 8oxoG-modified sequences—particularly 8oxo1—mirroring the
285 pattern of thermal destabilization. This suggests that the peptide bound preferentially to
286 the damaged base, possibly recognizing features specific to the damaged tetrad rather

287 than to the single nucleotide loop. Since CD spectra for these sequences showed minimal
288 changes in global topology, direct recognition of 8oxoG may drive this binding
289 preference.

290 In contrast, the AKKQ peptide bound similarly to all 8oxoG variants of the
291 $(GGGTT)_4$ sequence, which retained parallel conformations for most of the modifications.
292 The CD spectra revealed structural perturbations and decreased thermal stability of
293 8oxo1 and 8oxo5 (Fig 6C), but this had no influence on AKKQ binding. We attribute this
294 to the peptide having direct access to the intervening sequencing, supporting a ssDNA
295 loop targeting mechanism rather than direct 8oxoG recognition.

296 The telomeric G4 $(TTAGGG)_4$ was more conformationally dynamic, and again the
297 AKKQ peptide bound with the same affinity to both damaged and undamaged forms.
298 This is again consistent with the TTA ssDNA loops being more accessible to the peptide
299 in the hybrid and antiparallel configurations, allowing the FANCJ peptide to bind
300 directly to the loop rather than to the 8oxoG. Notably, in KCl, AKKQ binding to
301 $(TTAGGG)_4$ was approximately an order of magnitude stronger than for the other
302 sequences, but this distinction diminished in NaCl, except for the 8oxo5 variant, which
303 showed enhanced binding.

304 One possible explanation for the observed differences in binding preferences is
305 that high sodium concentrations affect the electrostatic interactions between the peptide
306 and the G4s. Sodium ions are known to provide less stabilization to G4s compared to

307 potassium [2-4]. We anticipated the FANCJ AKKQ peptide to adopt an alpha helical
308 structure due to previous NMR studies of the structurally and sequentially similar AKKQ
309 motif of the G4-binding protein RHAU [11]. Although our CD studies (Supporting
310 information) did not detect any alpha helical structure in either salt, the addition of
311 trifluoroethanol revealed a helical-like structure in both salt conditions. However, the
312 spectra obtained in each salt were not superimposable. This suggests that sodium ions
313 stabilize the peptide to a different extent than potassium ions.

314 Interestingly, the affinities of the AKKQ peptide for G4 DNA increased with loop
315 length, further supporting direct interactions with the ssDNA loop. Although FANCJ is
316 a helicase involved in DNA repair, our results suggest that the AKKQ binding site may
317 not function as a direct damage sensor but rather as a loop- or structure-selective binding
318 element. However, when the loop is too short to be recognized, FANCJ is able to target
319 the 8oxoG damage preferentially (Fig 11).

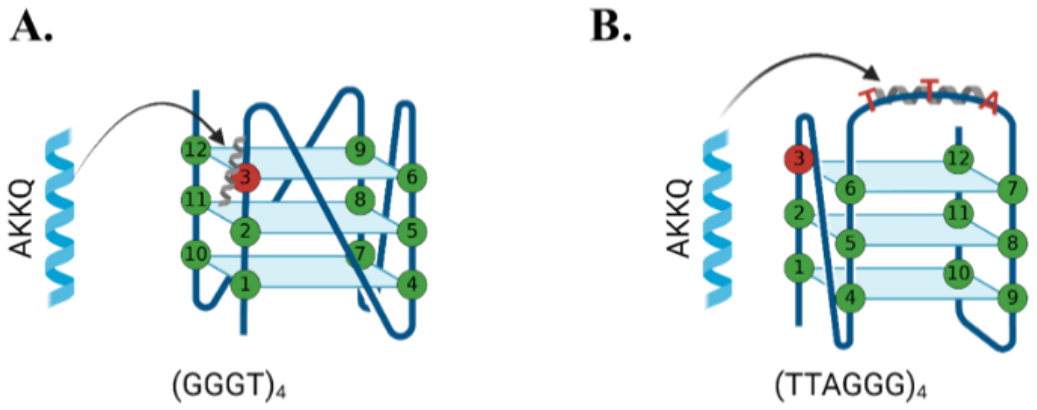

320

321 **Fig 11. Proposed binding interaction model between FANCJ AKKQ and 8oxoG4**
322 **sequences.** (A) For G4 sequences that form compact structures with short intervening
323 sequences, such as $(GGGT)_4$, AKKQ preferentially targets the 8oxoG site and promotes
324 repair. (B) For G4 sequences that expose the intervening sequence, as with antiparallel or
325 hybrid conformations, AKKQ preferentially targets the intervening sequence and ignores
326 the 8oxoG.

327 Biological implications and future directions

328 FANCJ is thought to coordinate with the translesion synthesis polymerase REV1
329 during replication of G4-rich regions [43]. It is plausible that FANCJ and REV1 perform
330 complementary roles, with FANCJ targeting conformationally dynamic G4s with
331 exposed loops, while REV1 preferentially targets the more compact and stable structures.
332 Exploring the G4-binding preferences and structural requirements of REV1 will be
333 essential to delineate their specialized activities during G4 remodeling.

334 This study examined 8oxoG substitutions at only three guanine positions. Future
335 studies should evaluate a broader set of damage positions, including systematic
336 substitutions across all tetrads, to determine whether the observed positional effects on
337 stability and recognition can be generalized. Additionally, incorporating full-length
338 FANCJ helicase for the binding studies instead of just the AKKQ G4-targeting site would

339 provide insights into whether other FANCJ domains participate in the recognition of
340 8oxoG4s.
341

342 Materials and methods

343 Buffers and reagents

344 All buffers were prepared with reagent-grade chemicals and Type I ultrapure
345 water from a Smart2Pure 6 UV/UF system (ThermoFisher, Waltham, MA). Solutions were
346 sterilized by filtration through 0.22 μm PES membranes prior to use.

347 Peptide and DNA oligos

348 FANCJ AKKQ peptide (129-PEKTTLAAKLSAKKQASIW-147) was synthesized
349 by Genscript (Piscataway, NJ), and the lyophilized powder was dissolved in 20 mM
350 HEPES pH 7.5, 150 mM KCl or NaCl, 5 mM TCEP, and 5% (v/v) glycerol. Peptide
351 concentration was determined using a NanoDrop One UV-Vis microvolume
352 spectrophotometer (ThermoFisher), based on the calculated molar extinction coefficients.
353 Peptides were aliquoted, frozen, and stored at -20 °C.

354 Oligodeoxyribonucleotides were purchased from Integrated DNA Technologies
355 (IDT, Coralville, IA). DNA concentrations were similarly measured by UV absorbance.

356 All oligonucleotides were stored at 4 °C. A list of the G4 DNA sequences used is provided

357 below in Table 5.

358 **Table 5. DNA Sequences.**

Name	Sequence (5′→3′)	Molar Extinction Coefficient ($M^{-1}cm^{-1}$)	Molecular Weight (g/mol)
$(GGGT)_4$	GGGTGGGTGGGTGGGT	157200	5105.3
$(GGGT)_4$ 8oxo1	T/i8oxodG/GGTGGGTGGGTGGGT	159100	5425.5
$(GGGT)_4$ 8oxo3	GG/i8oxodG/TGGGTGGGTGGGT	151600	5121.3
$(GGGT)_4$ 8oxo5	GGGTG/i8oxodG/GTGGGTGGGT	151600	5121.3
$(GGGTT)_4$	GGGTTGGGTTGGGTTGGGTT	189600	6322.1
$(GGGTT)_4$ 8oxo1	/i8oxodG/GGTTGGGTTGGGTTGGGTT	184000	6338.1
$(GGGTT)_4$ 8oxo3	GG/i8oxodG/TTGGGTGGGTTGGGTT	184000	6338.1

$(GGGTT)_4$ 8oxo5	GGGTTG/i8oxodG/GTTGGGTTGGGTT	184000	6338.1
$(TTAGGG)_4$	TTAGGGTTAGGGTTAGGGTTAGGG	244600	7575.0
$(TTAGGG)_4$ 8oxo1	TTA/i8oxodG/GGTTAGGGTTAGGGTTA GGG	239000	7590.9
$(TTAGGG)_4$ 8oxo3	TTAGG/i8oxodG/TTAGGGTTAGGGTTA GGG	239000	7590.9
$(TTAGGG)_4$ 8oxo5	TTAGGGTTAG/i8oxodG/GTTAGGGTTA GGG	239000	7590.9

CD spectroscopy

CD measurements were performed using a JASCO J-815 spectropolarimeter equipped with a PTC-423S Peltier temperature controller and a Koolance liquid cooling system. G4 samples were dialyzed into 20 mM boric acid containing either 150 mM KCl or NaCl. CD spectra were collected from 220 nm to 320 nm at 25 °C using 0.3 mg/mL DNA. Five traces per sample were averaged, and buffer baselines were subtracted.

For thermal denaturation experiments, samples were pre-heated to 95 °C and allowed to cool slowly overnight to 25 °C to ensure proper folding. Melting curves were recorded from 15 °C to 95 °C by monitoring the ellipticity at 262 nm (for parallel

368 conformations) or 295 nm (for antiparallel or hybrid structures). Three replicates were
369 performed for each experimental condition and the resulting data were averaged.

370 Melting temperatures (T_m) were determined in SigmaPlot using a two-state
371 transition model described by Greenfield [44], based on the Gibbs-Helmholtz equation:

372 $$\Delta G = \Delta H\left(1 - \frac{T}{T_m}\right) - \Delta C_p((T_m - T) + T\left(\ln\left(\frac{T}{T_m}\right)\right))$$

373 $$K = e^{(-\frac{\Delta G}{RT})}$$

374 $$y = \frac{K}{1 + K}$$

375 $$[\theta]_t = \left(([\theta]_F - [\theta]_U) * y\right) + [\theta]_U$$

376 where ΔG represents Gibbs free energy, ΔH represents enthalpy, ΔC_P represents the
377 change in heat capacity, K represents the folding constant, and y represents the fraction
378 of folded DNA at any given temperature, T. θ_t is the observed ellipticity at any
379 temperature, θ_F is the observed ellipticity of the folded DNA, and θ_U is the observed
380 ellipticity of the unfolded DNA. The melting temperature, T_m, of the DNA can then be
381 calculated as the temperature where y = 0.5.

382

383 **Fluorescence spectroscopy**

384 Fluorescence titration experiments were performed using a Cary Eclipse
385 Fluorescence Spectrophotometer (Agilent Technologies, Santa Clara, CA) equipped with
386 a PCB 1500 Peltier-controlled cuvette holder. Samples were exited at 280 nm, and the
387 emission spectra were collected from 300 to 450 nm at 25 °C.

388 A scan of buffer alone, 20 mM HEPES pH 7.5, 150 mM KCl or NaCl, 5 mM TCEP,
389 and 5% (v/v) glycerol, was used as a baseline. FANCJ AKKQ peptide (5 μM) was titrated
390 with additions of a DNA substrate. The mixture was allowed to equilibrate for 3 minutes
391 before taking each spectra scan.

392 Observed fluorescence quenching (ΔF) was calculated using the following
393 equation, with F_0 representing total fluorescence from the FANCJ peptide alone and F_i
394 representing the total fluorescence after the *i*th addition of DNA:

395 $$\Delta F = \frac{F_0 - F_i}{F_0}$$

396 Binding isotherms were calculated by plotting ΔF versus total DNA concentration.
397 The resulting curve was fit to a 1:1 interaction model using Scientist 2.0 software
398 (Micromath, St. Louis, MO) to calculate an equilibrium K. The equilibrium K was
399 calculated using the following formulas, where A was the amplitude of fluorescence
400 quenching and K was the equilibrium association constant. D_f and D_t were the free and
401 total concentration of DNA, while P_f and P_t described the free and total peptide

402 concentration. Fluorescence titrations were performed in triplicate. The reported K values

403 were determined from an average of three independent data-sets.

404
$$\Delta F_{obs} = A\left(\frac{KD_f}{1+KD_f}\right)$$
$$D_t = D_f(1+KP_f)$$
$$P_t = P_f(1+KD_f)$$

405 # Acknowledgements

406 Figs 1, 3-5, 8A, and 11 were created with BioRender.com.

407 # Author contributions

408 CGW designed experiments. LC, KL, and CGW acquired data and interpreted results.

409 LC, KL, EC, and CGW prepared the manuscript draft. All authors have read and agreed

410 to the published version of the manuscript.

411 # Financial disclosure statement

412 This work was supported by NSF CAREER grant 2142839 and AHA grant

413 17AIREA33661285 to CGW.

414 # Competing interests

415 Authors have no conflict of interest to disclose.

416 # References

417 1. Bochman ML, Paeschke K, Zakian VA. DNA secondary structures: stability and
418 function of G-quadruplex structures. Nature Reviews Genetics. 2012;13(11):770-
419 80.
420 2. Nový J, Böhm S, Králová J, Král V, Urbanová M. Formation and temperature
421 stability of G-quadruplex structures studied by electronic and vibrational circular
422 dichroism spectroscopy combined with ab initio calculations. Biopolymers.
423 2008;89(2):144-52.
424 3. Chaires JB. Human telomeric G-quadruplex: thermodynamic and kinetic studies
425 of telomeric quadruplex stability. The FEBS Journal. 2010;277(5):1098-106.
426 4. Guédin A, Gros J, Alberti P, Mergny J-L. How long is too long? Effects of loop size
427 on G-quadruplex stability Nucleic Acids Research. 2010;38(21):7858-68.
428 5. Huppert JL, Balasubramanian S. Prevalence of quadruplexes in the human
429 genome. Nucleic Acids Research. 2005;33(9):2908-16.
430 6. Lombardi EP, Holmes A, Verga D, Teulade-Fichou M-P, Nicolas A, Londoño-
431 Vallejo A. Thermodynamically stable and genetically unstable G-quadruplexes are
432 depleted in genomes across species Nucleic Acids Research. 2019;47(12):6098-113.

433 7. Hazel P, Huppert J, Balasubramanian S, Neidle S. Loop-length-dependent folding
434 of G-quadruplexes. Journal of the American Chemical Society. 2004;126(50):16405-
435 15.
436 8. Hao F, Ma Y, Guan Y. Effects of Central Loop Length and Metal Ions on the
437 Thermal Stability of G-Quadruplexes. Molecules. 2019;24(10).
438 9. Burge S, Parkinson GN, Hazel P, Todd AK, Neidle S. Quadruplex DNA:
439 sequence, topology and structure. Nucleic Acids Research. 2006;34(19):5402-15.
440 10. Villar-Guerra RD, Trent JO, Chaires JB. G-Quadruplex Secondary Structure
441 Obtained from Circular Dichroism Spectroscopy. Angewandte Chemie.
442 2018;57(24):7171-5.
443 11. Heddi B, Cheong VV, Martadinata H, Phan AT. Insights into G-quadruplex
444 specific recognition by the DEAH-box helicase RHAU: Solution structure of a
445 peptide–quadruplex complex. Proceedings of the National Academy of Sciences
446 of the United States of America. 2015;112(31):9608-13.
447 12. Budhathoki JB, Maleki P, Roy WA, Janscak P, Yodh JG, Balci H. A Comparative
448 Study of G-Quadruplex Unfolding and DNA Reeling Activities of Human RECQ5
449 Helicase. Biophysical Journal. 2016;110(12):2585-96.
450 13. Tippana R, Hwang H, Opresko PL, Bohr VA, Myong S. Single-molecule imaging
451 reveals a common mechanism shared by G-quadruplex–resolving helicases.

452 Proceedings of the National Academy of Sciences of the United States of America.
453 2016;113(30):8448-53.
454 14. Zheng K-W, Zhang J-Y, He Y-d, Gong J-Y, Wen C-J, Chen J-N, et al. Detection of
455 genomic G-quadruplexes in living cells using a small artificial protein. Nucleic
456 Acids Research. 2020;48(20):11706-20.
457 15. Wang L, Wang Q-M, Wang Y-R, Xi X-G, Hou X-M. DNA-unwinding activity of
458 Saccharomyces cerevisiae Pif1 is modulated by thermal stability, folding
459 conformation, and loop lengths of G-quadruplex DNA. Journal of Biological
460 Chemistry. 2018;293(48):18504-13.
461 16. Rhodes D, Lipps HJ. G-quadruplexes and their regulatory roles in biology Nucleic
462 Acids Research. 2015;43(18):8627-37.
463 17. Huppert JL, Balasubramanian S. G-quadruplexes in promoters throughout the
464 human genome. Nucleic Acids Research. 2006;35(2):406-13.
465 18. Beaudoin J-D, Perreault J-P. 5'-UTR G-quadruplex structures acting as
466 translational repressors. Nucleic Acids Research. 2010;38(20):7022-36.
467 19. Smith JS, Chen Q, Yatsunyk LA, Nicoludis JM, Garcia MS, Kranaster R, et al.
468 Rudimentary G-quadruplex-based telomere capping in Saccharomyces cerevisiae.
469 Nature Structural & Molecular Biology. 2011;18(4):478-85.

470 20. Georgakopoulos-Soares I, Parada GE, Wong HY, Medhi R, Furlan G, Munita R, et
471 al. Alternative splicing modulation by G-quadruplexes. Nature Communications.
472 2022;13(1).
473 21. Xu H, Di Antonio M, McKinney S, Mathew V, Ho B, O'Neil NJ, et al. CX-5461 is a
474 DNA G-quadruplex stabilizer with selective lethality in BRCA1/2 deficient
475 tumours. Nature Communications. 2017;8.
476 22. Steenken S, Jovanovic S. How Easily Oxidizable Is DNA? One-Electron Reduction
477 Potentials of Adenosine and Guanosine Radicals in Aqueous Solution. Journal of
478 the American Chemical Society. 1997;119(3):617-8.
479 23. Oikawa S. Sequence-specific DNA damage by reactive oxygen species:
480 Implications for carcinogenesis and aging. Environmental Health and Preventive
481 Medicine. 2005;10(2):65-71.
482 24. Neeley WL, Essigmann JM. Mechanisms of Formation, Genotoxicity, and
483 Mutation of Guanine Oxidation Products. Chemical Research in Toxicology.
484 2006;19(4):491-505.
485 25. Ohno M, Sakumi K, Fukumura R, Furuichi M, Iwasaki Y, Hokama M, et al. 8-
486 oxoguanine causes spontaneous de novo germline mutations in mice. Scientific
487 Reports. 2014;4.

488 26. Bielskutė S, Plavec J, Podbevšek P. Impact of Oxidative Lesions on the Human
489 Telomeric G-Quadruplex. Journal of the American Chemical Society.
490 2019;141(6):2594-603.
491 27. Vorlícková M, Tomasko M, Sagi AJ, Bednarova K, Sagi J. 8-oxoguanine in a
492 quadruplex of the human telomere DNA sequence. The FEBS Journal.
493 2012;279(1):29-39.
494 28. Jr RMB, Cantor SB. Molecular and cellular functions of the FANCJ DNA helicase
495 defective in cancer and in Fanconi anemia. Frontiers in Genetics. 2014;5.
496 29. Palovcak A, Liu W, Yuan F, Zhang Y. Maintenance of genome stability by Fanconi
497 anemia proteins. Cell & Bioscience. 2017;7.
498 30. Datta A, Robert M. Brosh J. Holding All the Cards—How Fanconi Anemia Proteins
499 Deal with Replication Stress and Preserve Genomic Stability. Genes. 2019;10(2).
500 31. Wu Y, Shin-ya K, Jr RMB. FANCJ helicase defective in Fanconia anemia and breast
501 cancer unwinds G-quadruplex DNA to defend genomic stability. Molecular and
502 Cellular Biology. 2008;28(12):4116-28.
503 32. Cantor SB, Xie J. Assessing the link between BACH1/FANCJ and MLH1 in DNA
504 crosslink repair. Environmental and Molecular Mutagenesis. 2010;51(6):500-7.
505 33. Sarkies P, Murat P, Phillips LG, Patel KJ, Balasubramanian S, Sale JE. FANCJ
506 coordinates two pathways that maintain epigenetic stability at G-quadruplex
507 DNA. Nucleic Acids Research. 2012;40(4):1485-98.

508 34. Bosch PC, Segura-Bayona S, Koole W, Heteren JTv, Dewar JM, Tijsterman M, et al.
509 FANCJ promotes DNA synthesis through G-quadruplex structures. The EMBO
510 Journal. 2014;33(21):2521-33.
511 35. Wu CG, Spies M. G-quadruplex recognition and remodeling by the FANCJ
512 helicase. Nucleic Acids Research. 2016;44(18):8742-53.
513 36. Lowran K, Campbell L, Popp P, Wu CG. Assembly of a G-Quadruplex Repair
514 Complex by the FANCJ DNA Helicase and the REV1 Polymerase. Genes.
515 2019;11(1).
516 37. Lattmann S, Giri B, Vaughn JP, Akman SA, Nagamine Y. Role of the amino
517 terminal RHAU-specific motif in the recognition and resolution of guanine
518 quadruplex-RNA by the DEAH-box RNA helicase RHAU. Nucleic Acids
519 Research. 2010;38(18):6219-33.
520 38. Rachwal PA, Fox KR. Quadruplex melting. Methods. 2007;43(4):291-301.
521 39. Do NQ, Lim KW, Teo MH, Heddi B, Phan AT. Stacking of G-quadruplexes: NMR
522 structure of a G-rich oligonucleotide with potential anti-HIV and anticancer
523 activity. Nucleic Acids Research. 2011;39(21):9448-57.
524 40. Guédin A, Cian AD, Gros J, Lacroix L, Mergny J-L. Sequence effects in single-base
525 loops for quadruplexes. Biochimie. 2008;90(5):686-96.
526 41. Lin C, Yang D. Human Telomeric G-Quadruplex Structures and G-Quadruplex-
527 Interactive Compounds. Methods in Molecular Biology. 2018:171-96.

42. Hardin CC, Watson T, Corregan M, Bailey C. Cation-dependent transition between the quadruplex and Watson-Crick hairpin forms of d(CGCG3GCG). Biochemistry. 1992;31(3):833–41.

43. Eddy S, Ketkar A, Zafar MK, Maddukuri L, Choi J-Y, Eoff RL. Human Rev1 polymerase disrupts G-quadruplex DNA. Nucleic Acids Research. 2014;42(5):3272-85.

44. Greenfield NJ. Using circular dichroism collected as a function of temperature to determine the thermodynamics of protein unfolding and binding interactions. Nature Protocols. 2006;1(6):2527-35.

Supporting information

S1 Fig. Experiments performed in the presence and absence of 20% (v/v) trifluoroethanol. (A) CD spectra of FANCJ AKKQ taken from 260 to 200 nm in the presence (blue) and absence (red) of trifluoroethanol in 150 mM KCl. (B) CD Spectra of FANCJ AKKQ taken from 260 to 200 nm in the presence (black) and absence (gray) of trifluoroethanol in 150 mM NaCl. Upon the addition of trifluoroethanol in either salt condition, an alpha helical conformation appears.